Chemical and architectural intricacy from nanoscale tetrahedra and their analogues

Jeremy Schneider, Yasutaka Nagaoka, Hongyou Fan,* and Ou Chen*

The tetrahedron, as the simplest platonic shape, is a profound building block with the potential to create intricate superstructures. Noteworthy designs utilizing tetrahedral building blocks include the Sierpiński tetrahedron (the most fundamental three-dimensional fractal), a one-dimensional helical structure known as the tetrahelix, and various crystalline and quasicrystalline packings. Historically, the practicality of tetrahedral superstructures has been evident, providing stable, well-defined frameworks for various constructions, including truss bridges, tower cranes, and electricity transmission line pylons. In the field of self-assembled nanocrystal superlattices, tetrahedral nanocrystals, as building blocks, occupy a unique place among all the possible nanoscale particles. Mathematical models, simulation work, and experimental studies using nanocrystals in the laboratory have suggested that self-assembled structures derived from nanoscale tetrahedral building blocks are notably intricate, giving rise to new horizons of high-entropy nanocrystal superlattices. An important implication from previous works is that such tetrahedral nanocrystal superlattices form through highly delicate interparticle interactions, emphasizing the importance of the fine features of these nanocrystals. In this article, we summarize the advances in superlattices assembled from tetrahedral nanocrystals. We first define the tetrahedron and tetrahedron analogues based on Conway's transformation and graph theory, underscoring their relevance to the crystallization process producing tetrahedral nanocrystals. Then, we showcase previous reports on the synthesis of tetrahedral nanocrystals and the resulting nanocrystal superstructures. Finally, we conclude by offering insights and perspective into the chemical and architectural intricacy that could emerge from tetrahedral nanocrystals.

Introduction

The tetrahedron is the simplest of Platonic solids, and its iconic shape has influenced the art, philosophy, engineering, and science of many cultures worldwide. The ancient Greek philosopher Plato associated the tetrahedron with the element of fire, as its sharp, penetrating points are reminiscent of the heat and transformative power of fire.[1] Da Vinci's tetrahedron stars, compounds of two regular tetrahedra, were investigated by notable researchers and artists including Johannes Kepler and Luca Pacioli.[1] In stark contrast to the simplicity of the tetrahedron shape, superstructures of tetrahedra exhibit profound complexity, which has been recognized by researchers in various fields across many eras. Notably, the packing problem of tetrahedra has been debated since antiquity.[2–5] Ever since Aristotle's claim that tetrahedra could completely fill space had proven incorrect, there has been an exciting scientific journey to find the densest packings of tetrahedra.[2–6] The champion structures, as of this publication, are those proposed by E.R. Chen et al., which possess a packing density of 85.63% with a striking quasicrystal-related arrangement.[5] Another fascinating example of tetrahedral superstructure is the Sierpiński tetrahedron; the fractal superstructure is created from tetrahedral building blocks connected through the vertices.[7] This three-dimensional (3D) fractal structure is also known to have an integral number of two in its Hausdorff dimension—an extremely rare case in fractal structures.[7] Besides, tetrahedra-based superstructures have proven to be functional in many capacities. For example, truss structures in

Jeremy Schneider, Department of Chemistry, Brown University, Providence, USA; Jeremy_schneider@brown.edu
Yasutaka Nagaoka, Department of Chemistry, Brown University, Providence, USA; yasuyasu@brown.edu
Hongyou Fan, Sandia National Laboratories, Albuquerque, USA; hfan@sandia.gov
Ou Chen, Department of Chemistry, Brown University, Providence, USA; ouchen@brown.edu
*Corresponding author
doi:10.1557/s43577-024-00688-8

bridges and towers are among the greatest inventions throughout history, enabling robust architectures supported by tetrahedron frameworks.[8]

In the field of nanocrystal (NC) self-assembly, researchers have been attracted to the shape of tetrahedra, which could potentially result in, for example, the creation of dissipative systems and advancing self-assembled NC systems to the next level.[9–15] The concept of dissipative systems in self-assembly was notably developed by I. Prigogine.[16] In such cases, dissipative self-assemblies can flexibly alter their structures in an open thermodynamic system, as seen in many dynamic living organisms.[11,16] While most conventional NC superlattices (SLs) are thermodynamically constrained,[9] the geometrical complexity of tetrahedra-based superstructures increases the entropy of the systems, bringing the structures one step closer to the flexibility level required by any dissipative systems.[6,10,11,16] Indeed, recent research has shown that a few high-entropy structures can be attained from self-assemblies of tetrahedral NC building blocks, including tetrahedral helical structures,[13] conventional crystalline and unconventional quasicrystalline and its approximant SLs,[12,17,18] as well as non-Euclidean superstructures that relieved geometrical frustration through intricate assembly behaviors.[17,19]

A critical insight derived from previous self-assembly research of tetrahedral NCs is that the architectural intricacy in NC SLs can be realized only when multiple desired conditions are met.[11,13,17,20] In the early stage, only relatively simple and localized superstructures were possible from assembled tetrahedral-shaped NCs.[21] However, subsequent research, fueled by refined synthetic methods of nano-tetrahedrons, revealed that details such as self-assembly conditions, surface states, and truncation levels of the building blocks are key to achieving high-entropy superstructures.[11–13] With a firm belief in the adage "God is in the details," this article discusses the fine experimental aspects that lead to sophisticated superstructures possible from tetrahedral and tetrahedral-like NCs. We first discuss the shape of the tetrahedron and its analogues using Conway's transformation and graph theory, offering comprehensive shape arguments in a simple manner. Then, we showcase tetrahedral NC-based superstructures reported to date, emphasizing the synthetic procedures of the building blocks and the experimental conditions for self-assembly. We discuss the detailed shapes of NC inorganic cores, the surface profiles, and the interparticle interactions induced by the experimental conditions in self-assembly. In conclusion, we offer our perspectives on tetrahedral NC SLs in the broader context of self-assembly research, laying the groundwork toward the future generation of NC superstructures.

Tetrahedron and tetrahedron analogues: An overview using graph theory

NCs shaped like tetrahedra and their analogues have been produced from various materials, including metals, metal chalcogenides, and metal pnictogens.[21–28] Researchers have developed NC synthetic methods to finely control features of the resulting tetrahedral-like shapes, including truncation at the edges and vertices, as well as the curvature of the facets, and other tetrahedron-related shapes such as tetrahedral frames and tetrapods.[29–35] Discussing these shape irregularities is crucial for the self-assembly process, yet a comprehensive showcase of these tetrahedral shape deviations is challenging due to the large number of variables, necessitating a simplified discussion. We employ graph theory and Conway's transformation operators to address the irregularities often observed in synthesized tetrahedral-like NCs. Graph theory offers a simplified approach by focusing on vertices and edges, allowing an overview of a complete set of tetrahedron analogues and an understanding of their properties.[36] Conway's operators provide a comprehensive set of transformations that tetrahedral NCs can undergo.[37] As a model study, we examine three transformation processes commonly observed in NC systems—edge-truncated, vertex-truncated, and twisted tetrahedra.

A tetrahedron, with its four vertices, four faces, and six edges, is depicted in graph theory as a triangle divided into three smaller triangles (**Figure 1**, left). When all four vertices are truncated, the tetrahedron eventually transforms into an octahedron, a transformation known as "Ambo" according to Conway's operators (Figure 1a). This transformation has been observed in NC syntheses; for example, a cubic-phase-based tetrahedral crystal with four {111} facets undergoes vertex truncation upon the emergence of the other four {111} facets.[22] Edge transformations are realized through the "Chamfer" operation in Conway's transformations, which converts the edge line into a hexagonal plane (Figure 1b), corresponding to {100} facet exposure in the cubic crystal system.[22] Last, the "Snub" operation introduces chirality, resulting in an intermediate twisted tetrahedral shape with 20 triangular faces, followed by further twisting to form a regular icosahedron as shown in the two-dimensional (2D) graph and 3D model in Figure 1c.

Mechanisms of tetrahedral NC growth and origins of Conway truncations

Recent studies focusing on the dynamics of NC growth have provided crucial details to explain how tetrahedral NCs form, despite often featuring morphologies deviating from the symmetry of their underlying crystal structures.[28,29,38–40] These studies provide clues to the formation of common Conway truncations on tetrahedral NC surfaces (e.g., Ambo and Chamfer truncations), as well as to less common Snub truncation of Ag_{70} clusters (**Figure 2**a–b).[41] Interestingly, the symmetry breaking and particle growth processes of tetrahedral-like NCs are highly dependent on underlying crystal structure. For example, an investigation of the growth modes of zinc-blende (ZB) InP NCs unveiled a two-step particle growth process.[28] The initial growth along four {111} facets produced intermediate tetrapod structures, followed by a subsequent overgrowth step along the exposed {110} facets to produce well-formed and highly uniform tetrahedra (Figure 2c–d).[28] The authors

notably extracted the differential activation energy barriers for monomer addition to {111} and {110} facets of ZB InP NCs based on temperature-controlled growth experiments. The calculation results revealed that the higher activation barrier for growth along {110} facets facilitated the controlled synthesis of tetrapodal and tetrahedral NCs by adjusting temperatures during the final growth step. In this case, Ambo truncations could be explained as the original ends of the intermediary tetrapodal legs, which exhibit {111} surface exposure just like the faces of the overall tetrahedron in the final NC. The kinetic findings, particularly regarding the separation of {111} and {110}-facet-directed growth modes, explain why Ambo truncations remain throughout the entire growth process; growth on these exposed facets terminates after the initial tetrapodal growth step to yield final tetrahedrons with full coverage of {111} crystal planes.

In contrast, a study by the M. Jones group investigating Au NCs with a face-centered-cubic (fcc) crystal structure demonstrated that symmetry breaking from the O_h seeds to T_d NCs proceeded via an anisotropic growth process.[38] In this process, monomer addition to the surface of the Au NCs gradually changed the exposed facets from {100} to {111} via a series of high-index {hh1} crystal facets (Figure 2e–f). *In situ* liquid cell transmission electron microscopy (TEM) measurements tracked the shape evolution of single NCs during the growth, observing the transition from {110}-capped seeds to {111}-capped Au tetrahedral NCs.[38] Similar to the ZB InP tetrahedral NC case previously discussed, the M. Jones group concluded that the transition from the higher-energy {110}-capped surface to the {111}-capped surface of the tetrahedron was energetically favorable in the presence of surface ligands with amine head groups (i.e., cetyltrimethylammonium bromide, CTAB). In this case, the higher surface area of {110} facets again explains the preference of Ambo truncation for cubic systems, as this form of truncation yields NCs that still are fully capped by {111} facets while reducing high-surface energy regions often found at areas of high curvature (e.g., vertices).

One example from the O. Chen group was unique in terms of a striking surface profile and high uniformity of size and shape of the tetrahedral-like CdSe/CdS core/shell quantum dot (QD) NCs.[40] The synthesized NCs possessed 8.4-nm crystal height with a 2.3-nm truncation along the edges.[40] Unlike most previous examples of tetrahedral NCs, this system produced truncated tetrahedral NCs from the CdSe seeds with a noncubic wurtzite (WZ) crystal structure. The WZ crystal structure possesses inherent crystal polarity, with a highly elongated *c*-axis, and tetrahedral-like WZ NCs therefore exhibit asymmetric surface exposure rather than complete exposure of {111} facets as for systems with cubic crystal structures. Instead, three $\{10\bar{1}1\}$ facets and one {0002} facet should be exposed on the tetrahedral-like WZ CdSe/CdS core/shell QD NCs (Figure 2g).[40] Interestingly, the truncation of these NCs is not vertex-directed Ambo truncation as is ubiquitous for cubic systems; rather, Chamfer truncation of the vertical edges is present, yielding hexagonal pyramidal NCs when "fully" truncated such that all six vertical faces are identical. These results are in line with the results from cubic systems, as Chamfer truncation for WZ crystals yields a similar result as Ambo truncation for cubic systems; namely, the formation of NCs with crystallographically symmetric facets and truncation surfaces. In the case of WZ NCs, Chamfer truncation is preferred owing to the sixfold symmetry of the $\{10\bar{1}1\}$ facets, which causes Chamfer truncations to occur along three $\{10\bar{1}1\}$ crystal planes and results in NCs capped by six $\{10\bar{1}1\}$ facets and one basal {0002} facet. In all the previously discussed cases, shape truncations are present to reduce surface energy by minimizing overall shape sharpness (truncating vertices and edges of tetrahedron), while retaining full surface exposure of energetically favorable crystal planes (i.e., {111} for cubic systems, and $\{10\bar{1}1\}$ for hexagonal systems).

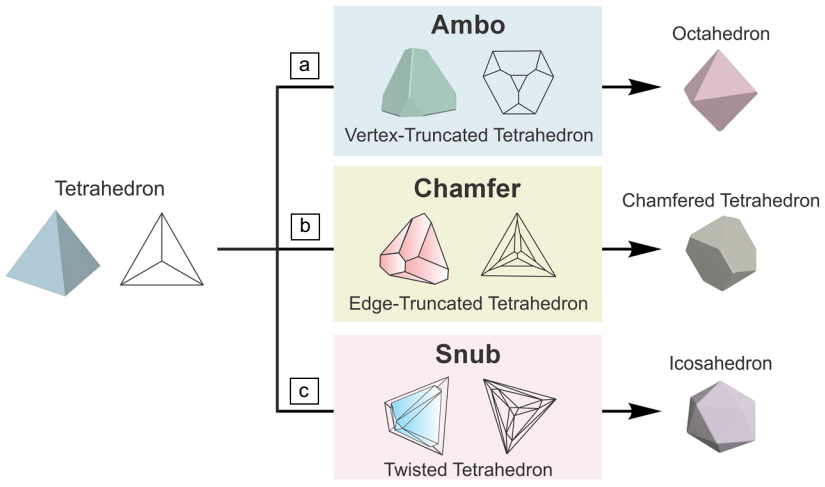

Figure 1. Three-dimensional models and graph theory presentations of a tetrahedron (left), "Ambo" operation (vertex-truncated) (a), "Chamfer" operation (edge-truncated) (b), and "Snub" operation (twisted tetrahedron) (c) in Conway's transformations.

Intricate superstructures assembled from tetrahedral NCs

Monolayer and localized self-assembly of tetrahedral NCs

Early self-assembly research largely investigated relatively simple structures, in which a single layer of NCs

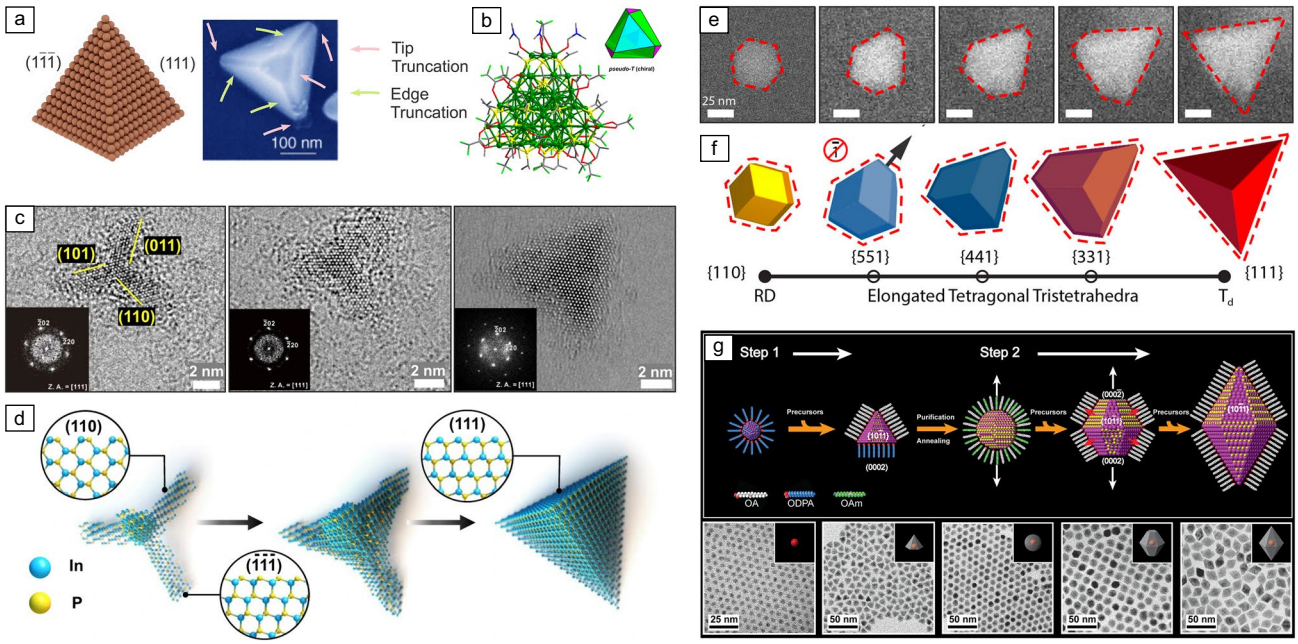

Figure 2. Growth mechanisms for tetrahedral and tetrahedral-like nanocrystals (NCs). (a) Computer model of tetrahedral NC with four {111} faces (left), and scanning electron microscopy image of an Au tetrahedral NC with vertex (pointed with pink arrows) and edge (pointed with green arrows) truncations (right). Adapted with permission from Reference 29. © 2004 Wiley-VCH. (b) Atomic model of twisted tetrahedral Ag_{70} cluster. Three-dimensional model of the cluster geometry (inset). Adapted with permission from Reference 41. © 2022 Springer Nature. (c) Transmission electron microscopy (TEM) images of InP NC undergoing {110} overgrowth from tetrapodal (left) to tetrahedral (right) morphology. Adapted with permission from Reference 28. © 2021 Springer Nature. (d) Three-dimensional models representing tetrapodal (left), {110} overgrowing (center), and tetrahedral (right) NCs. Adapted with permission from Reference 28. (e) TEM images of Au NC undergoing shape transformation from cubic seed (left) to tetrahedral NC (right). Adapted with permission from Reference 38. © 2021 American Chemical Society. (f) Three-dimensional models of Au NC undergoing shape transformation from cubic seed (left) to tetrahedral NC (right), with major surface facet labeled. Adapted with permission from Reference 38. (g) Three-dimensional models (top) of spherical CdSe quantum dot (QD) NCs undergoing successive growth steps to tetrahedral and hexagonal bipyramidal CdSe/CdS core/shell QD NCs; the corresponding TEM images of the growth process (bottom). Adapted with permission from Reference 40. © 2017 American Chemical Society. RD, rhombic dodecahedron; T_d, tetrahedral.

deposited on a support substrate to form either monolayer SLs with periodicities, or local organized cluster units.[42–45] Similar to self-assembly of spherical NCs, the earliest cases of tetrahedral NC self-assembly obtained hexagonal monolayers, yet with striking orientational orders for the NCs within these SLs. For example, the studies on tetrahedral NC self-assembly, published by Z. Wang et al. in 1997 and 1998, identified two forms of orientational order.[46,47] When 4.4-nm CoO tetrahedral NCs with a ZB crystal phase were assembled via the evaporation of toluene solvent on a TEM grid, measurement results revealed long-range orientational alignments parallel to the viewing direction (i.e., perpendicular to the plane of the TEM grid).[46] When viewed from this projection, the synthesized tetrahedral NCs, exposed with only {111} facets, were found to universally orient vertex-up on the TEM grid such that the [110] direction of each NC was oriented perpendicular to the plane of the SL (**Figure 3**a–c).[48] The same group later studied the toluene evaporative self-assembly of 4.5-nm Ag tetrahedral NCs with vertex-directed Ambo truncations, and found the same long-range orientational alignments, with additional rotational ordering around the [110] crystal axis in a short range.[47] For small domains (up to ~50 nm), high-resolution (HR) TEM measurements revealed that NCs oriented around the [110] axis such that their surface ligands maximally intercalated and filled the inter-NC space (Figure 3c–d). This orientational pattern requires two facet-to-facet connections and one vertex-to-facet connection per NC, with an interesting consequence that the resulting structure loses the sixfold symmetry present in SLs formed from spherical NCs. Given that the inter-NC distance is greater for vertex-to-facet connections than facet-to-facet connections, the displayed assembly pattern is effectively stretched in one dimension relative to a corresponding sixfold lattice.

L. Manna et al. showed another example of SLs from tetrahedral-like NCs exhibiting unique interparticle interactions.[49] In this study, they used WZ CdSe QD NCs with edge lengths of 20.3 nm and 16 nm for axial and basal edges, respectively.[49] The WZ CdSe tetrahedral-like NCs were synthesized through a one-pot hot-injection method using CdO, $CdCl_2$, and Se powder as precursors, and octadecylphosphonic acid (ODPA) as the capping ligand.[49] The exposed facets consisted of one $\{0002\}_{WZ}$ and three $\{40\bar{4}5\}_{WZ}$ facets, and

overall shape was roughly tetrahedral with compression in the *c*-direction. Interestingly, clover-shaped cluster-type units were formed upon solvent evaporation (Figure 3e). From TEM, clover units with each consisting of four CdSe NCs were visualized, indicating strong attractions between $\{40\bar{4}5\}_{WZ}$ facets of WZ CdSe NCs. Such directional interactions arose from differences of surface ligand density between $\{0002\}_{WZ}$ facets and $\{40\bar{4}5\}_{WZ}$ facets, and directional crystal polarity along the *c*-directions, with the important implication that tetrahedral NC building blocks can translate such delicate directional interactions into complex superstructure formation. In 2018, Q. Zhang et al. produced a highly similar localized superstructure using core–shell Au/Ag right bipyramidal NCs featuring distorted tetrahedral shape (Figure 3f).[50] In both cases, patchy ligand–ligand interactions were implicated in the nonentropic, non-close-packed assembly of novel structures from tetrahedral-like NCs with flat, prominent surface facets and high vertex and edge curvatures.

Large-scale multilayer SLs: Developing principles for surface-directed self-assembly of tetrahedral NCs

A seminal work reported by the Talapin group, outlining the first successful self-assembly of tetrahedral CdSe QD NCs into a large-scale 3D SL, provided new conceptual depth to models of tetrahedral NC packing.[51] While the superstructure obtained was relatively simple, the forces underpinning the interparticle interactions were distinct from conventional SLs. In this study, the authors used 8- and 10-nm ZB CdSe tetrahedral NCs with oleic acid or stearic acid as the tethering ligands.[51] For the formation process, they employed a slow solvent evaporation method from tetrachloroethylene, which facilitated formation of a multilayer superstructure (**Figure 4**a). Their TEM studies revealed a hexagonal lattice, with alternating rotational orientation of adjacent NCs (Figure 4b–e). The interpretations of these findings drew on earlier work investigating self-assembly of octahedral NCs, which found that those NCs preferentially assembled into a non-close-packed body-centered-cubic (bcc) structure under equilibrium conditions.[52] Of key interest was the observation from TEM imaging that this octahedron-based superstructure was dominated by vertex-to-vertex connections between adjacent NCs, rather than the facet-to-facet connections predicted by entropy.[52,53] Similarly, Talapin et al. found that their tetrahedral NCs formed a multilayer SL with particle orientations maximizing vertex-to-vertex connections even at the entropic cost of lower packing fraction (Figure 4b–e). This phenomenon was ascribed to a dynamic evolution of surface

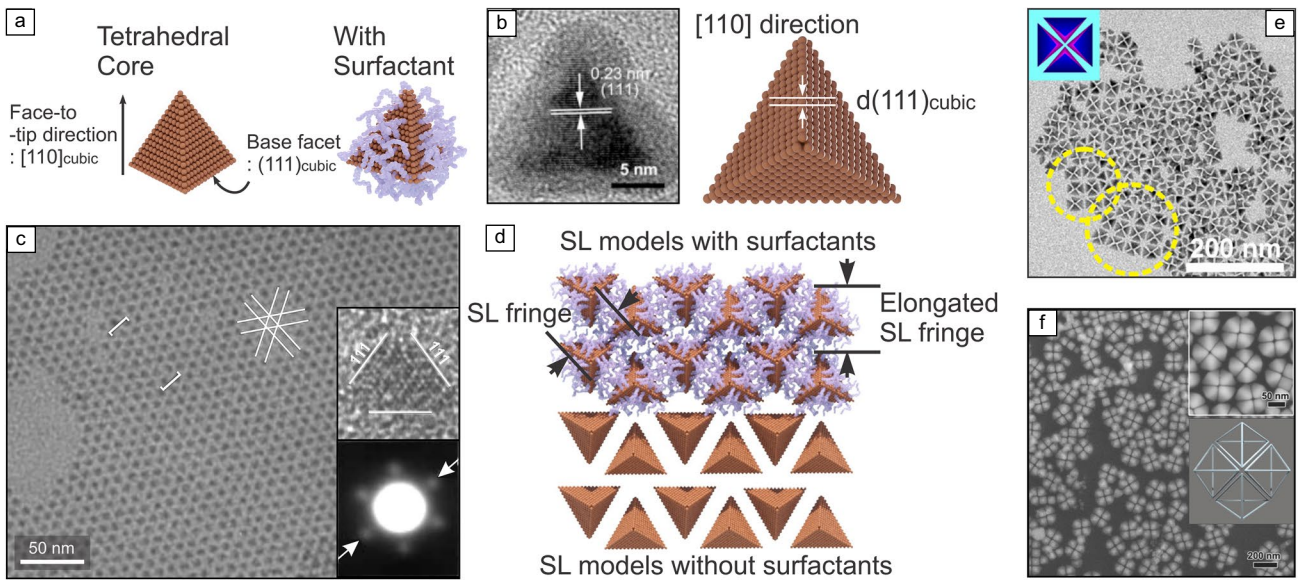

Figure 3. Characterization of tetrahedral nanocrystal (NC) surfaces and early superlattices (SLs) assembled from tetrahedral NCs. (a) Three-dimensional models of tetrahedral NC core (left) and surface ligand (right) profiles. Arrow at left indicates alignment of the tetrahedral morphology such that the vertex of the tetrahedron is aligned with the [110] direction of the cubic crystal structure. (b) High-resolution transmission electron microscopy (HR-TEM) image of a tetrahedral Pd NC, emphasizing the surface (111) facet coverage (left). Adapted with permission from Reference 48. © 2011 Wiley-VCH. Model of the tetrahedral NC viewed from the [110] crystal direction (right). (c) TEM image of self-assembled Ag tetrahedral NCs demonstrating hexagonal connectivity and short-range orientational order. High-resolution TEM image of single NC (inset, top), and small-angle electron diffraction pattern of superlattice (inset, bottom). Adapted with permission from Reference 47. © 1998 Wiley-VCH. (d) Proposed model for explaining the observed orientational alignment of adjacent NCs. (e) TEM image and model (inset) of short-range clover superstructures formed upon self-assembly of CdSe compressed tetrahedral NCs, displaying selective facet-to-facet connectivity. Adapted with permission from Reference 49. © 2015 American Chemical Society. (f) TEM image, HR-TEM image (inset, top), and 3D model (inset, bottom) of short-range clover superstructures formed upon self-assembly of Au/Ag right bipyramidal NCs. Adapted with permission from Reference 50. © 2018 Wiley-VCH.

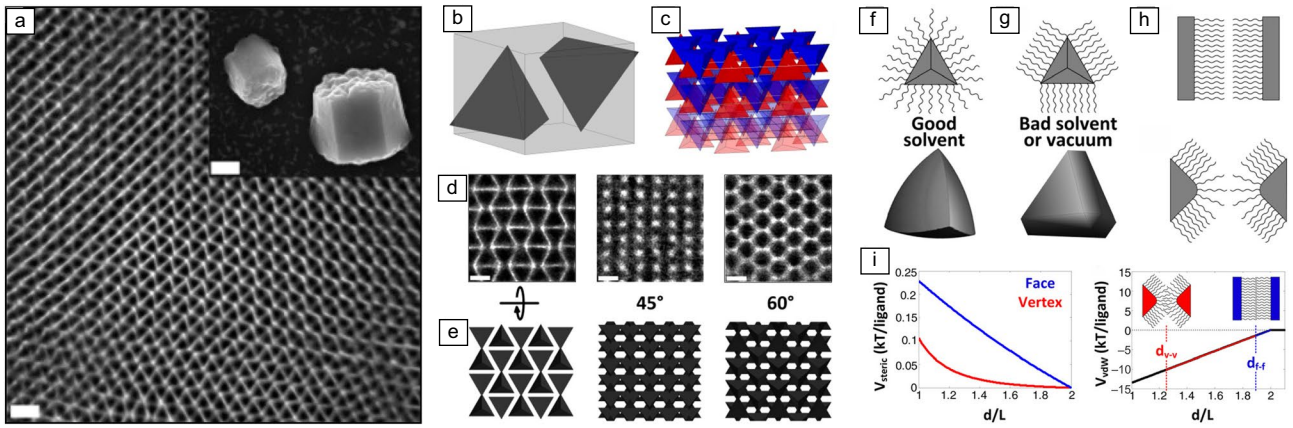

Figure 4. Three-dimensional structure formed from tetrahedral nanocrystals (NCs) exhibiting asymmetric surface ligand attractive forces. (a) Large-scale transmission electron microscopy (TEM) image of superlattices (SLs) formed upon by tetrahedral CdSe NCs (scale bar = 20 nm). Scanning electron microscopy image of supercrystals (inset, scale bar = 1 μm). Adapted with permission from Reference 51. (b) Unit cell of 3D crystal structure. Adapted with permission from Reference 51. © 2014 American Chemical Society. (c) Three-dimensional model of SL, colored to represent two possible NC orientations. Adapted with permission from Reference 51. (d) TEM images of 3D NC SL produced by evaporative self-assembly of 8-nm tetrahedral CdSe NCs, viewed from the [110] projection (left) and rotated around the $(110)_{SL}$ axis for visualization of the cubic crystal structure (center) and hexagonal NC packing (right). Adapted with permission from Reference 51. (e) Models of the 3D NC SL, viewed from the [110] projection (left) and rotated around the $(110)_{SL}$ axis for visualization of the cubic crystal structure (center) and hexagonal NC packing (right). Adapted with permission from Reference 51. (f) Two-dimensional (top) and 3D (bottom) models of the ligand corona of CdSe NCs when dispersed in favorable (good) solvent such as toluene. Adapted with permission from Reference 51. (g) Two-dimensional (top) and 3D (bottom) models of the ligand corona of CdSe NCs upon evaporation of solvent. Adapted with permission from Reference 51. (h) Two-dimensional models of surface ligand intercalation at NC facets (top) and vertices (bottom). Adapted with permission from Reference 51. (i) Repulsive steric forces between adjacent NC surfaces while dispersed in solvent (left) and attractive van der Waal's forces between adjacent NC surfaces after evaporation (right).

ligand configuration during the assembly process, termed an "effective patchiness" effect.[51] When suspended in favorable (good) solvent, surface-bound oleic acid molecules mixed with solvent molecules and puffed to produce an effective NC shape resembling a rounded tetrahedron (Figure 4f). Upon evaporation of the solvent, the surface ligand puffs bundled more tightly and behaved similar to the rigid, straight models described in earlier self-assembly works,[46] with an associated effective shape change to a cantellated tetrahedron with high ligand density on NC facets (Figure 4g).

The authors associated the high density of vertex-to-vertex connections with the increased surface curvature at vertices relative to facets, allowing for increased intercalation of surface ligands on adjacent NCs (Figure 4h). As the solvent evaporated during the assembly process, these attractive ligand–ligand intercalation effects drove local particle orientations to prefer vertex-to-vertex, rather than less attractive facet-to-facet, connectivity (Figure 4i). Effectively, the vertices with lower ligand density functioned as attractive patches for the attachment of adjacent NCs. Therefore, the researchers concluded that ligand–ligand enthalpic contributions were on par with entropic space-packing considerations in determining the end superstructure. Furthermore, the results for the study provided valuable clues regarding the kinetics of the evaporative self-assembly process for anisotropic NCs. The striking resemblance of the obtained SL to simulated results for puffy hard particles indicate that short-range orientational alignment of nearby NCs could take place while still suspended in solution or at the solvent-substrate interface, pointing toward a key role for both surface ligands and solvent molecules in mediating superstructures formed during colloidal self-assembly processes.[2,51]

Self-assembly of tetrahedral NCs into complex crystalline and quasicrystalline SLs

The role of surface ligand patchiness in driving tetrahedral NC self-assembly was further elaborated by a set of discoveries published by the O. Chen group in 2018, which reported a wide variety of SLs assembled from tetrahedral-like CdSe/CdS core/shell QD NCs (previously presented).[12,13] Importantly, these NCs possessed a hexagonal WZ crystal structure, and therefore exposed two different types of crystal facets with anisotropic surface ligands coverage: oleic acid tethered $\{10\bar{1}1\}$ facets and ODPA passivated {0002} facet (**Figure 5**a),[40] owing to their distinct ligand affinities to the different exposed WZ crystal facets.[12,13,40] Assembling these tetrahedral-like NCs with anisotropic surface patchiness resulted in complex superstructures featuring from one-dimensional (1D), 2D, and 3D NC connectivity.[13] Specifically, 1D helices, 2D "zip/log unit-based" lattices, and 3D cluster-based lattices were formed via evaporative self-assembly on solid substrates (Figure 5b–d).[13] Remarkably, the first reported single-component quasicrystalline NC SL was then observed by the O. Chen group when the evaporative self-assembly process occurred

with liquid ethylene glycol as the substrate.[18] The critical role of surface ligand patchiness for promoting self-assembly of complex superstructures from tetrahedral NCs was demonstrated by the formation mechanism discussed in these works.[12,13] The anisotropic surface ligand coverage promoted a strong orientational bias, where the ODPA-coated {0002} facets of adjacent NCs preferentially faced toward each other to form dimerized building units. These dimers can then be either assembled into helical or crystalline SL structures on a solid substrate depending on the applied NC solution concentration,[13] or further coordinated into short-range flexible decagonal units, which finally form long-range tenfold quasicrystalline domains following the proposed "flexible polygon tiling rule" (Figure 5e).[12] Assembly mechanistic studies confirmed the criticality of both anisotropic surface patchiness and tetrahedral-like shape of the NCs for obtaining the described low-packing fraction phase. Significantly, these results furthered the recognition of substrate identity as a crucial determinant of the end superstructure. The tenfold quasicrystalline lattices could not be obtained from self-assembly processes occurring on solid substrates such as carbon-coated TEM grids or silicon wafers.[18] Moreover, precise matching of liquid substrates to solvent and surface ligands was also a requirement for quasicrystal formation. Under standard experimental conditions using cyclohexane as the dispersing solvent and oleic acid/ODPA as surface ligands, only self-assembly occurring on the surface of an ethylene glycol subphase produced quasicrystalline structures, with self-assembly on substrates with higher or lower polarities yielding only other crystalline phases. In line with past results, the existence of a substrate effect indicates that self-assembly is initiated at the solvent-substrate interface rather than in the bulk of the solvent or following complete solvent evaporation.[51] Therefore, these results can be used to extend existing models of tetrahedral self-assembly even farther by holistically including solvent-ligand and substrate–ligand interactions as driving forces for final SL structures.

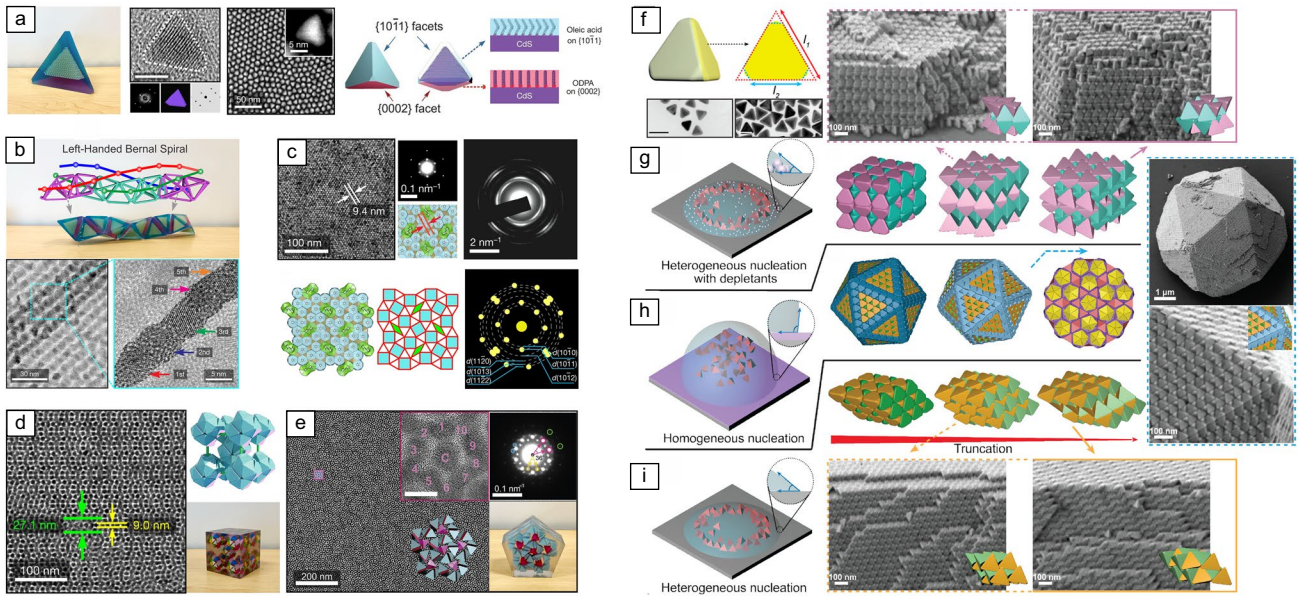

Figure 5. Complex crystalline and quasicrystalline superlattices (SLs) formed from tetrahedral nanocrystals (NCs). (a) Three-dimensional printed model of CdSe/CdS core/shell tetrahedral quantum dot NC (left); high-resolution transmission electron microscopy (HR-TEM) (center left) and dark-field TEM (center right) images, adapted with permission from Reference 13. © 2018 Springer Nature; schematics demonstrating anisotropic surface coverage (right). Adapted with permission from Reference 18. © 2022 Elsevier. (b) Three-dimensional printed model of chiral tetrahelix (top); TEM (bottom left) and HR-TEM (bottom right) images of self-assembled 1D tetrahelices. Adapted with permission from Reference 13. (c) TEM image of sixfold quasicrystal-approximant SL (top left), with small-angle electron diffraction and computer model of SL (top center), and wide-angle electron diffraction (top right); computer models of SL assembled by zip/log units (bottom left) and simulated wide-angle electron diffraction (bottom right). Adapted with permission from Reference 13. (d) TEM image of 3D cluster-based back-centered-cubic (bcc) SL (left); computer (top right) and 3D printed (bottom right) models of a cluster-based bcc unit cell. Adapted with permission from Reference 13. (e) TEM image of tenfold single-component quasicrystalline SL (left); HR-TEM image of decagonal unit (top inset) and 3D model of local packing order (bottom inset); small-angle electron diffraction displaying tenfold symmetry (top right); 3D printed model of local packing order (bottom right). Adapted with permission from Reference 12. © 2018 AAAS. (f) Three-dimensional model of truncated tetrahedral Au NCs, with projection demonstrating truncation extent (top); TEM images of Au tetrahedral NCs (bottom). Adapted with permission from Reference 17. © 2023 American Chemical Society. (g) Superstructures formed during heterogeneous assembly of Au NCs in the presence of depletants. Adapted with permission from Reference 17. (h) Superstructures formed during homogeneous assembly of Au NCs. Adapted with permission from Reference 17. (i) Superstructures formed during heterogeneous assembly of Au NCs without depletants. Adapted with permission from Reference 17.

Recently, X. Ye et al. reported another quasicrystalline SL from tetrahedral Au NCs with structural complexity.[17] The authors employed refined seeded-growth methods to synthesize tetrahedral Au NCs that enabled fine control over the Ambo truncation level of the vertices (Figure 5f). The NCs exhibited excellent size and shape uniformity with an average size of 70 nm, capped by 11-mercaptoundecanoic acid and cetyltrimethylammonium chloride (CTAC) surface ligands. Homogeneous self-assembly of such tetrahedral NCs suspended in water yielded 3D supercrystals with dodecagonal quasicrystalline symmetry in two dimensions and periodic, layer-by-layer stacking of the dodecagonal units in the third dimension.[17] Interestingly, the cases of quasicrystal formation from tetrahedral NCs reported by both groups were accompanied by reports of various crystalline structures (Figure 5b–d, g–i). In the case of truncated Au tetrahedrons, modification of assembly conditions again changed end superstructures. However, precisely controlled differences in vertices' truncation (i.e., Ambo truncation) were also shown to affect SL structures. When truncation extent was systematically varied under different assembly conditions, nearly ten different superstructures were generated with varying levels of orientation alignment as well as translational periodicity.[17,21] In addition to shape effects stemming from vertex truncation of the NCs, the authors additionally found evidence that assembly conditions drove the self-assembly processes toward different end structures.[17,21] Similar to the findings by the O. Chen group in which environmental conditions such as substrate and solvent identity affected the final superstructure,[12,13] X. Ye et al. found that substrate replacement, which modified the assembly process from homogeneously occurring in the bulk of the solvent to heterogeneously happening at the solvent-substrate interface, drastically changed which structures formed from similar NC populations.[17,21] Addition of depletants (i.e., CTAC) also impacted the assembly process, modifying the obtained SLs from hexagonal diamond phases (in the absence of depletants) to cubic diamond phases (in the presence of depletants).[17]

Self-assembly of tetrahedral NCs into chiral systems

Outside of quasicrystal formation from tetrahedral NCs, the Kotov group has pioneered superstructures with various chemical and structural intricacies using truncated tetrahedral CdTe QD NCs.[54–58] In 2002, the group began using CdTe tetrahedral NCs with Ambo truncation along the vertices for self-assembly into complex superstructures.[54] The CdTe NCs showed strong fusing ability on the exposed facets, which transformed the long-range SLs into fused thin nanosheets (**Figure 6**a–b).[55] Recently, the authors produced CdTe NCs coated with chiral cysteine as the surface ligands, which acted as a templating agent for the directed assembly of enantiopure tetrahelices with controllable chirality (Figure 6c).[56] The Kotov group also produced similar helices using light as a stimuli for the assembly of racemic tetrahelices,[57] later additionally discovering that circularly polarized light was capable of biasing resulting tetrahelix chirality by up to 30 percent.[58] The assembled helices exhibited controllable chiroptical properties across an astonishing range of wavelengths (ca. 300–1300 nm), with optical responses altering in response to modified helical pitch (Figure 6d).[56] A theoretical background was later established for these results,[19] which incorporated the earlier idea regarding ligand–ligand interactions while additionally providing a sophisticated geometric rationale related to the inability of tetrahedrons to completely pack 3D space. In this model, ligand coronas act as flexible linkers permitting rotation of tetrahedral NC cores around connective axes between adjacent particles (Figure 6e). In this way, the tetrahedrons can relieve geometric frustrations associated with nonunity tiling patterns.[19,56] This theory was applied to justify the high incidence of lower-dimensional structures formed from tetrahedral NCs, as higher-dimensional structures such as 3D supercrystals lose rotational freedom on the single-particle level in exchange for more attractive enthalpic connections between NC surface ligands.

In 2022, the M. Jones group reported another striking, yet simple, example of chiral structures from Au tetrahedral NCs.[59] They produced Au NCs with a size of 66.3 nm, capped with positively charged CTAC and dispersed in water. Upon evaporation of the solvent, the NCs formed a final structure determined by a balance of van der Waals interactions between NC cores, repulsive electrostatic interactions from CTAC ligands, and depletion forces.[59] As a result, hexagonal "pinwheel" local ordering, in which two layers of NCs form on a flat substrate with alternating polarity along the vertical axis and a tilt angle in the horizontal dimension up to 22º (Figure 6f). Due to the horizontal tilt of adjacent NCs, this structure exhibited racemic chirality on the large scale, with left-handed and right-handed enantiomers defined by positive or negative tilts. The authors ascribed this remarkable structure to the delicate balance between entropy and surface ligand-based enthalpic effects; in this case, repulsive electrostatic interactions between positively charged CTAC molecules promoted an abundance of vertex-to-edge connections, rather than the expected edge-to-edge or facet-to-facet connections that would result in a more close-packed "honeycomb" structure (Figure 6g–h).[59] Later in the same year, the Q. Chen group reported another example of chiral structures from Au Ambo-truncated tetrahedral NCs.[60] Their Au NCs with a size range of ca. 32 nm–68 nm formed remarkably similar chiral pinwheels upon evaporation of aqueous solvent (Figure 6i–j). Photon-induced near-field electron microscopy (PINEM), finite-difference time-domain (FDTD) simulations, and circular dichroism measurements were used to model and measure the chiroptical properties of the assembled pinwheel SLs.[60] The authors found that the optical responses were dependent on the chiral twist angle as well as the domain size of the measured SL, and

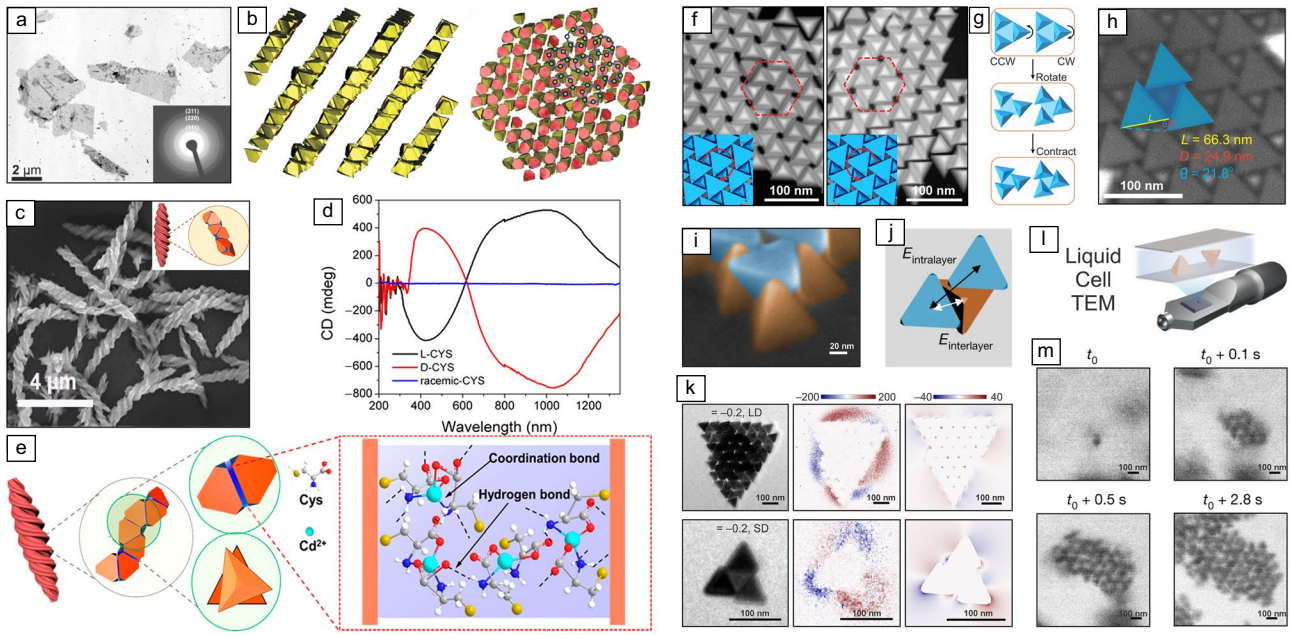

Figure 6. Chiral superstructures assembled from tetrahedral nanocrystals (NCs). (a) Transmission electron microscopy (TEM) image of nanosheets assembled from fused CdTe tetrahedral quantum dot (QD) NCs. Adapted with permission from Reference 55. © 2006 AAAS. (b) Three-dimensional models demonstrating local packing of NCs within nanosheets from the side (left) and top (right). Adapted with permission from Reference 55. (c) Scanning electron microscopy (SEM) image of chiral twisted ribbons formed from bundles of tetrahelices. Three-dimensional model of twisted ribbon, with close-up to individual tetrahelix unit (inset). Adapted with permission from Reference 56. © 2020 American Chemical Society. (d) Circular dichroism (CD) spectrum for solutions of twisted ribbons, color-coded for solutions with L-, D-, and racemic-cysteine surface ligands. Adapted from Reference 56. (e) Three-dimensional model of twisted ribbon (left), with close-up views to individual tetrahelix units from side (center top) and top (center bottom) views, and atomic model of cysteine interactions between adjacent NCs (right). Adapted from Reference 56. (f) SEM images of left-handed (left) and right-handed (right) pinwheel superlattices (SLs), with 3D models (insets). Adapted with permission from Reference 59. © 2022 Springer Nature. (g) Formation mechanism of chiral pinwheel structures from achiral units. CW, clockwise; CCW, counterclockwise. Adapted with permission from Reference 59. (h) SEM images of pinwheel SLs, overlaid with a 3D model demonstrating NC size, displacement, and tilt angle. Adapted with permission from Reference 59. (i) SEM image of Au tetrahedral NCs within pinwheel SL. Adapted with permission from Reference 60. © 2022 Springer Nature. (j) Three-dimensional model displaying interparticle forces for bilayer assemblies of tetrahedral NCs. Adapted with permission from Reference 60. (k) SEM images of large-scale (left, top) and small-scale (left, bottom) pinwheel assemblies with identical chiral twist angles, with corresponding photon-induced near-field electron microscopy data (center) and finite-difference time-domain simulations (right). LD, large domain; SD, small domain. Adapted with permission from Reference 60. (l) Computer model of liquid cell TEM setup for *in situ* measurements. Adapted with permission from Reference 60. (m) Time-resolved snapshots of pinwheel self-assembly process, taken *in situ* using liquid cell TEM. Adapted with permission from Reference 60.

therefore highly tunable simply through small modifications to the Au NC shape via Ambo truncations, or assembly conditions (Figure 6k). *In situ* TEM imaging allowed dynamic characterization of the formation processes of the pinwheel structures (Figure 6l–m).[60] Their observations also support the model of chiral pinwheel superstructures forming based on a delicate thermodynamic equilibrium between surface ligand repulsions and entropic close-packing biases. Interestingly, the authors additionally ascribed geometric frustrations to the formation of the 2D planar structures rather than 3D supercrystals, arguing again that the inability of tetrahedrons to completely fill space in three dimensions biased assembly processes toward lower-dimensional structures, which incorporated complex structural elements such as chiral twists to relieve remaining packing frustrations.[19,59,60]

Coda

Researchers in the NC self-assembly field have long been in pursuit of functional superstructural nanomaterials, extending beyond fundamental studies. This quest embraces diverse objectives, ranging from achieving structured materials with specific functions to emulating out-of-equilibrium states seen in biological systems.[10,11,61–63] The findings highlighted in this article underscore the distinctive role that nanoscale tetrahedral and tetrahedral-analogue particles could play in advancing these goals. By investigating the assemblies of tetrahedral-type NCs at various levels from geometrical arrangement to entropic and enthalpic states, one can harness structural and property information that is inaccessible through the study of NC superstructures of other types.[64–71]

Recent dedicated efforts in tetrahedral-type NC self-assembly have advanced the field forward since the initial reports of monolayer or localized superstructures.[46,47,49] Notably, our conceptual understanding of the forces governing tetrahedral NC self-assembly has evolved from basic 2D models explaining short-range orientational alignments to sophisticated 3D structures incorporating ligand-involved effective shapes and interparticle interactions.[13,17–19,21,51] These models play a crucial role in elucidating the intricacies of dynamic assembly processes, with the aim of transcending the constrains of current knowledge and progress into comprehensive frameworks that consider a myriad of determining factors such as NC and surface ligand interactions, solvent and substrate effects, geometric considerations, and external forces. Fortunately, prior experimental observations, theoretical insights and their convergence have successfully demonstrated the feasibility of precise control and characterization of these aspects influencing tetrahedral NC self-assembly.[29,38,40,41,72–76]

Despite growing recognition of the importance of tetrahedral-type NC self-assembly, a universal set of design principles encompassing a holistic approach for systematically tuning the assembly samples to obtain desired superstructures remain elusive. Consequently, the vast potential of the nanoscale tetrahedron and its analogues as structural and functional building blocks is yet to be fully realized. As the library of tetrahedron-based SLs expands while researchers continue refining the system, we expect that ongoing efforts will gradually narrow existing gaps in our understanding of tetrahedral self-assembly. This progress should ultimately allow us not only to predict end SL structures with knowledge of relevant parameters, but also to design superstructural nanomaterials for the next generation, bridging both fundamental sciences and practical applications. In short, the devoted efforts in the field of tetrahedral-type NC self-assembly have already laid a solid foundation, placing the field in a position where it "stands on the shoulders of giants." We eagerly anticipate forthcoming advancements from such a vaunted position in the near future.

Conflict of interest

On behalf of all authors, the corresponding authors state that there is no conflict of interest.

Author contributions

J.S., Y.N., and O.C. wrote the manuscript. All authors commented on and edited the manuscript.

Funding

O.C. acknowledges the support from the National Science Foundation through Award No. DMR-1943930. O.C. also acknowledges supports from the Camille & Henry Dreyfus Foundation through the Camille Dreyfus Teacher-Scholar Award program and the Alfred P. Sloan Foundation through the Sloan Research Fellowship Award program. Sandia National Laboratories is a multimission laboratory managed and operated by National Technology and Engineering Solutions of Sandia, LLC, a wholly owned subsidiary of Honeywell International, Inc., for the US DOE's National Nuclear Security Administration (Contract No. DE-NA-0003525). The views expressed in the article do not necessarily represent the views of the US DOE or the US government.

Data availability

Not available.

References

1. H. Coxeter, *Regular Polytopes* (Dover Publications, Mineola, 1973)
2. Y. Kallus, V. Elser, *Phys. Rev. E* **83**, 036703 (2011)
3. S. Torquato, Y. Jiao, *Nature* **460**, 876 (2009)
4. J.H. Conway, S. Torquato, *Proc. Natl. Acad. Sci. U.S.A.* **103**, 10612 (2006)
5. E.R. Chen, M. Engel, S.C. Glotzer, *Discrete Comput. Geom.* **44**, 253 (2010)
6. A. Haji-Akbari, M. Engel, A.S. Keys, X. Zheng, R.G. Petschek, P. Palffy-Muhoray, S.C. Glotzer, *Nature* **462**, 773 (2009)
7. H. Tsuiki, Projected images of the Sierpinski tetrahedron and other fractal imaginary cubes (2023), Preprint, arXiv:2205.13065
8. J.C. Wallach, L.J. Gibson, *Int. J. Solids Struct.* **38**, 7181 (2001)
9. M.A. Boles, M. Engel, D.V. Talapin, *Chem. Rev.* **116**, 11220 (2016)
10. B.A. Grzybowski, W.T.S. Huck, *Nat. Nanotechnol.* **11**, 585 (2016)
11. M. Yang, H. Chan, G. Zhao, J.H. Bahng, P. Zhang, P. Král, N.A. Kotov, *Nat. Chem.* **9**, 287 (2017)
12. Y. Nagaoka, H. Zhu, D. Eggert, O. Chen, *Science* **362**, 1396 (2018)
13. Y. Nagaoka, R. Tan, R. Li, H. Zhu, D. Eggert, Y.A. Wu, Y. Liu, Z. Wang, O. Chen, *Nature* **561**, 378 (2018)
14. G.M. Whitesides, B. Grzybowski, *Science* **295**, 2418 (2002)
15. G. Makey, S. Galioglu, R. Ghaffari, E.D. Engin, G. Yıldırım, Ö. Yavuz, O. Bektaş, Ü.S. Nizam, Ö. Akbulut, Ö. Şahin, K. Güngör, D. Dede, H.V. Demir, F.Ö. Ilday, S. Ilday, *Nat. Phys.* **16**, 795 (2020)
16. W.C. Schieve, P.M. Allen (eds.), *Self-Organization and Dissipative Structures: Applications in the Physical and Social Sciences* (University of Texas Press, Austin, 1982)
17. Y. Wang, J. Chen, R. Li, A. Götz, D. Drobek, T. Przybilla, S. Hübner, P. Pelz, L. Yang, B. Apeleo Zubiri, E. Spiecker, M. Engel, X. Ye, *J. Am. Chem. Soc.* **145**(32), 17902 (2023)
18. Y. Nagaoka, J. Schneider, H. Zhu, O. Chen, *Matter* **6**, 30 (2023)
19. F. Serafin, J. Lu, N. Kotov, K. Sun, X. Mao, *Nat. Commun.* **12**, 4925 (2021)
20. C.B. Murray, C.R. Kagan, M.G. Bawendi, *Annu. Rev. Mater. Sci.* **30**, 545 (2000)
21. Y. Wang, J. Chen, Y. Zhong, S. Jeong, R. Li, X. Ye, *J. Am. Chem. Soc.* **144**, 13538 (2022)
22. H. Zhang, M. Jin, Y. Xia, *Angew. Chem. Int. Ed.* **51**, 7656 (2012)
23. C. Burda, X. Chen, R. Narayanan, M.A. El-Sayed, *Chem. Rev.* **105**, 1025 (2005)
24. P. Zhao, N. Li, D. Astruc, *Coord. Chem. Rev.* **257**, 638 (2013)
25. A.N. Beecher, X. Yang, J.H. Palmer, A.L. LaGrassa, P. Juhas, S.J.L. Billinge, J.S. Owen, *J. Am. Chem. Soc.* **136**, 10645 (2014)
26. A.R. Tao, S. Habas, P. Yang, *Small* **4**, 310 (2008)
27. Z. Zhuang, Q. Peng, X. Wang, Y. Li, *Angew. Chem. Int. Ed.* **46**, 8174 (2007)
28. Y. Kim, H. Choi, Y. Lee, W. Koh, E. Cho, T. Kim, H. Kim, Y.-H. Kim, H.Y. Jeong, S. Jeong, *Nat. Commun.* **12**, 4454 (2021)
29. F. Kim, S. Connor, H. Song, T. Kuykendall, P. Yang, *Angew. Chem. Int. Ed.* **43**, 3673 (2004)
30. N. Mishra, V.G. Vasavi Dutt, M.P. Arciniegas, *Chem. Mater.* **31**, 9216 (2019)
31. L. Manna, E.C. Scher, A.P. Alivisatos, *J. Am. Chem. Soc.* **122**, 12700 (2000)
32. M. Haddadnezhad, W. Park, I. Jung, H. Hilal, J. Kim, S. Yoo, Q. Zhao, S. Lee, J. Lee, S. Lee, S. Park, *ACS Nano* **16**, 21283 (2022)
33. J. Park, A. Oh, H. Baik, Y.S. Choi, S.J. Kwon, K. Lee, *Nanoscale* **6**, 10551 (2014)
34. D. Li, X. He, M. Su, Y. Zhao, J. Li, T. Huang, H. Liu, *RSC Adv.* **7**, 37938 (2017)
35. X. Huang, S. Tang, H. Zhang, Z. Zhou, N. Zheng, *J. Am. Chem. Soc.* **131**, 13916 (2009)
36. J. Harris, J. Hirst, M. Mossinghoff, *Combinatorics and Graph Theory*, 2nd edn. (Springer, New York, 2008)
37. J. Conway, H. Burgiel, C. Goodman-Strauss, *The Symmetries of Things*, 1st edn. (CRC Press, Boca Raton, 2008)
38. M. Sun, Z. Cheng, W. Chen, M. Jones, *ACS Nano* **15**(10), 15953 (2021)
39. Z. Zhao, Z. Sun, H. Zhao, M. Zheng, P. Du, J. Zhao, H. Fan, *J. Mater. Chem.* **22**, 21965 (2012)
40. R. Tan, Y. Yuan, Y. Nagaoka, D. Eggert, X. Wang, S. Thota, P. Guo, H. Yang, J. Zhao, O. Chen, *Chem. Mater.* **29**, 4097 (2017)

41. X.-M. Luo, C.-H. Gong, F. Pan, Y. Si, J.-W. Yuan, M. Asad, X.-Y. Dong, S.-Q. Zang, T.C.W. Mak, *Nat. Commun.* **13**, 1177 (2022)
42. M.D. Bentzon, J. van Wonterghem, S. Mørup, A. Thölén, C.J.W. Koch, *Philos. Mag. B* **60**, 169 (1989)
43. C.J. Brinker, Y. Lu, A. Sellinger, H. Fan, *Adv. Mater.* **11**, 579 (1999)
44. C.B. Murray, C.R. Kagan, M.G. Bawendi, *Science* **270**, 1335 (1995)
45. G. Bailey, R. Dimlich, K. Alexander, J. McCarthy, T. Pretlow, S.A. Harfenist, Z.L. Wang, R.L. Whetten, I. Vezmar, M.M. Alvarez, B.E. Salisbury, *Microsc. Microanal.* **3**, 431 (1997)
46. J.S. Yin, Z.L. Wang, *Phys. Rev. Lett.* **79**, 2570 (1997)
47. Z.L. Wang, S.A. Harfenist, I. Vezmar, R.L. Whetten, J. Bentley, N.D. Evans, K.B. Alexander, *Adv. Mater.* **10**(10), 808 (1998)
48. Z. Niu, Q. Peng, M. Gong, H. Rong, Y. Li, *Angew. Chem. Int. Ed.* **50**, 6315 (2011)
49. S. Ghosh, R. Gaspari, G. Bertoni, M.C. Spadaro, M. Prato, S. Turner, A. Cavalli, L. Manna, R. Brescia, *ACS Nano* **9**, 8537 (2015)
50. F. Ji, Q. Zhong, J. Chen, L. Chen, H. Hu, Q. Liu, P. Yang, J. Yu, L. Jiang, Y. Xu, E. Gross, Q. Zhang, *Part. Part. Syst. Charact.* **35**, 1700114 (2018)
51. M.A. Boles, D.V. Talapin, *J. Am. Chem. Soc.* **136**, 5868 (2014)
52. J. Zhang, Z. Luo, Z. Quan, Y. Wang, A. Kumbhar, D.-M. Smilgies, J. Fang, *Nano Lett.* **11**(7), 2912 (2011)
53. J. Henzie, M. Grünwald, A. Widmer-Cooper, P.L. Geissler, P. Yang, *Nat. Mater.* **11**, 131 (2012)
54. Z. Tang, N.A. Kotov, M. Giersig, *Science* **297**, 237 (2002)
55. Z. Tang, Z. Zhang, Y. Wang, S.C. Glotzer, N.A. Kotov, *Science* **314**, 274 (2006)
56. J. Yan, W. Feng, J.-Y. Kim, J. Lu, P. Kumar, Z. Mu, X. Wu, X. Mao, N.A. Kotov, *Chem. Mater.* **32**, 476 (2020)
57. S. Srivastava, A. Santos, K. Critchley, K.-S. Kim, P. Podsiadlo, K. Sun, J. Lee, C. Xu, G.D. Lilly, S.C. Glotzer, N.A. Kotov, *Science* **327**, 1355 (2010)
58. J. Yeom, B. Yeom, H. Chan, K.W. Smith, S. Dominguez-Medina, J.H. Bahng, G. Zhao, W.-S. Chang, S.-J. Chang, A. Chuvilin, D. Melnikau, A.L. Rogach, P. Zhang, S. Link, P. Král, N.A. Kotov, *Nat. Mater.* **14**, 66 (2015)
59. Z. Cheng, M.R. Jones, *Nat. Commun.* **13**, 4207 (2022)
60. S. Zhou, J. Li, J. Lu, H. Liu, J.-Y. Kim, A. Kim, L. Yao, C. Liu, C. Qian, Z.D. Hood, X. Lin, W. Chen, T.E. Gage, I. Arslan, A. Travesset, K. Sun, N.A. Kotov, Q. Chen, *Nature* **612**(7939), 259 (2022)
61. K. Bian, H. Schunk, D. Ye, A. Hwang, T.S. Luk, R. Li, Z. Wang, H. Fan, *Nat. Commun.* **9**, 2365 (2018)
62. Y. Zhong, Z. Wang, R. Zhang, F. Bai, H. Wu, R. Haddad, H. Fan, *ACS Nano* **8**, 827 (2014)
63. Y. Tian, J.R. Lhermitte, L. Bai, T. Vo, H.L. Xin, H. Li, R. Li, M. Fukuto, K.G. Yager, J.S. Kahn, Y. Xiong, B. Minevich, S.K. Kumar, O. Gang, *Nat. Mater.* **19**, 789 (2020)
64. Y. Zhong, J. Wang, R. Zhang, W. Wei, H. Wang, X. Lü, F. Bai, H. Wu, R. Haddad, H. Fan, *Nano Lett.* **14**, 7175 (2014)
65. L. Fang, J.Y. Park, Y. Cui, P. Alivisatos, J. Shcrier, B. Lee, L.-W. Wang, M. Salmeron, *J. Chem. Phys.* **127**, 184704 (2007)
66. M. De Giorgi, D. Tarì, L. Manna, R. Krahne, R. Cingolani, *Microelectronics J.* **36**, 552 (2005)
67. R. Narayanan, M.A. El-Sayed, *J. Phys. Chem. B* **108**, 5726 (2004)
68. G. Barbillon, A. Ivanov, A.K. Sarychev, *Symmetry* **12**, 896 (2020)
69. Y. Zhou, M. Califano, *J. Phys. Chem. Lett.* **12**, 9155 (2021)
70. R. Narayanan, M.A. El-Sayed, *J. Am. Chem. Soc.* **126**, 7194 (2004)
71. Q. Zhou, G. Jiang, *Chem* **4**, 2022 (2018)
72. H. Kim, N.T. Khi, J. Yoon, H. Yang, Y. Chae, H. Baik, H. Lee, J.-H. Sohn, K. Lee, *Chem. Commun.* **49**, 2225 (2013)
73. P.F. Damasceno, M. Engel, S.C. Glotzer, *Science* **337**, 453 (2012)
74. P.F. Damasceno, M. Engel, S.C. Glotzer, *ACS Nano* **6**, 609 (2012)
75. R. van Damme, G.M. Coli, R. van Roij, M. Dijkstra, *ACS Nano* **14**, 15144 (2020)
76. W. Jin, P. Lu, S. Li, *Sci. Rep.* **5**, 15640 (2015) □

Jeremy Schneider is a doctoral candidate in the Department of Chemistry at Brown University. He received his BS degree in chemistry from Stony Brook University, The State University of New York, in 2017, and his MAT degree in chemistry education from Stony Brook University in 2018, where he investigated chemical content knowledge of prospective chemistry teachers across the United States. His research focuses on self-assembly of anisotropic nanocrystals into exotic crystalline and quasicrystalline superlattices. Schneider can be reached by email at Jeremy_schneider@brown.edu.

Yasutaka Nagaoka is a research assistant professor in the Department of Chemistry at Brown University. He received his BS and MS degrees in chemistry from Keio University, Japan, where he researched photoresponsive materials and developed a system using boron-doped diamond for arsenic electrochemical detection. He received his PhD degree in chemistry from the University of Florida. His current research focuses on self-assembly and high-pressure chemistry of nanocrystals. Nagaoka can be reached by email at yasuyasu@brown.edu.

Hongyou Fan received a BS degree in chemistry from Jilin University, a MS degree from the Chinese Academy of Sciences in polymer science, and a PhD degree in chemical engineering from The University of New Mexico. He was a postdoctoral fellow at Sandia National Laboratories before working there full-time. He currently is the head of the Geochemistry Department, the US Department of Energy Office of Science Basic Energy Sciences Sandia Geoscience program manager, and a distinguished member of the Technical Staff at Sandia National Laboratories. His current research focuses on fundamental understanding of interfacial processes of nanoscale colloids for synthesis and integration of functional nanomaterials. Fan can be reached by email at hfan@sandia.gov.

Ou Chen is an associate professor in the Department of Chemistry at Brown University. He received his BS degree in chemical physics from the University of Science and Technology of China, in 2004 and completed his PhD study in the Department of Chemistry at the University of Florida. After postdoctoral training at the Massachusetts Institute of Technology, he joined Brown University in the fall of 2015. His current research interests focus on exploring novel methodologies for fabrications of functional nanocrystals, semiconductor quantum dots, perovskite nanomaterials, and their self-assembled higher-order superstructures for optical, catalysis, and energy-related applications. Chen can be reached by email at ouchen@brown.edu.